Polymer 51 (2010) 3887–3898

Contents lists available at ScienceDirect

Polymer

journal homepage: www.elsevier.com/locate/polymer

Synthesis and characterization of sulfonated polyimides bearing sulfonated aromatic pendant group for DMFC applications

Fei Sun, Taipeng Wang, Shiyong Yang, Lin Fan*

Laboratory of Advanced Polymer Materials, Institute of Chemistry, Chinese Academy of Sciences, Zhongguancun, Beijing 100190, China

ARTICLE INFO

Article history:
Received 22 April 2010
Received in revised form
30 May 2010
Accepted 2 June 2010
Available online 9 June 2010

Keywords:
Sulfonated polyimides
Proton conductivity
Methanol permeability

ABSTRACT

A novel side-chain-type sulfonated aromatic diamine, 5-[1,1-bis(4-aminophenyl)-2,2,2- trifluoroethyl]-2-(4-sulfophenoxy)benzenesulfonic acid (BABSA) was synthesized and characterized. Two series of sulfonated polymides (SPI-N and SPI-B) were prepared from 1,4,5,8-naphthalene tetracarboxylic dianhydride (NTDA) or 4,4′-binaphthyl-1,1′,8,8′-tetracarboxylic dianhydride (BNTDA), sulfonated diamine BABSA and various non-sulfonated aromatic diamines. The resulting sulfonated polyimide (SPI) membranes exhibited good dimensional stability with isotropic swelling of 7–22% and high thermal stability with desulfonation temperature of 283–330 °C. These membranes also displayed excellent oxidation stability and good water stability. The SPI membranes exhibited better permselectivity than Nafion 115 membrane due to their much lower methanol permeability. The ratios of proton conductivity to methanol permeability (Φ) for the SPI membranes were almost two to three times of that for Nafion 115. The SPI-N membranes exhibited excellent conducting performance with the proton conductivity higher than Nafion 115 as the temperature over 40 °C, which attributed to their good hydrophobic/hydrophilic microphase separation structure.

1. Introduction

Direct methanol fuel cell (DMFC) has been considered as the ideal fuel cell system since it produces electric power by direct conversion of the methanol fuel at the fuel cell anode [1,2]. The advantages of DMFC, such as high energy density, convenient fuel supply, quick start times, and instant refueling, make it more attractive as mobile and portable power sources for cell phones, notebook computers and other electronic devices [3,4]. A proton exchange membrane with high conductivity and good stability is one of the most important components in a DMFC system. The perfluorosulfonic acid polymer membranes, such as Nafion membranes, are the most successfully applied polymeric materials for DMFC due to their high proton conductivity, good mechanical property and excellent chemical stability [5,6]. However, their drawbacks, including high costs, low operation temperature and high methanol crossover, have to be overcome in commercial applications [7–11].

In the past decades, many kinds of sulfonated aromatic polymers have been developed as the alternative proton exchange membrane materials, such as poly(ether ether ketone)s [12–14], poly(ether sulfone)s [15,16], polybenzimidazoles [17] and polyimides [18–21]. They are expected to have low methanol crossover and high proton conductivity. Among these sulfonated aromatic polymers, sulfonated polyimides (SPIs) are recognized as one of the most promising alternative materials for fuel cell applications due to their excellent combination properties of high thermal stability, excellent mechanical strength, superior chemical resistance, good film forming ability as well as significantly low methanol permeability [22–25]. However, common five-membered ring polyimides are generally unstable toward acid due to the ease of hydrolysis of imide rings.

Mercier and his coworkers first successfully developed sulfonated polyimides from a six-membered ring dianhydride 1,4,5,8-naphthalenetetracrboxylic dianhydride (NTDA), which replaced the five-membered ring dianhydrides, a commercially available sulfonated diamine 2,2-benzidinedisulfonic acid (BDSA) and common non-sulfonated diamines [26,27]. They found that the NTDA-based SPI membranes showed reasonably high performance in a H_2/O_2 fuel cell system and the hydrolysis stability was greatly improved by incorporation of naphthalenic imide structures. However, the proton conductivities of these membranes were rather low due to their low ion exchange capacity (IEC), which limited their further development for applications.

In recent years, many kinds of sulfonated polyimides based on NTDA and novel sulfonated aromatic diamines have been developed to improve the proton conducting performance. It is known

* Corresponding author. Tel.: +86 10 6256 4819; fax: +86 10 6256 9562.
E-mail address: fanlin@iccas.ac.cn (L. Fan).

0032-3861/$ – see front matter © 2010 Elsevier Ltd. All rights reserved.
doi:10.1016/j.polymer.2010.06.005

that SPIs can be classified into main-chain-type and side-chain-type. In the former, the sulfonic acid groups are bonded directly to the polymer backbones, while in the latter, they are attached to the side chains of the polymer [28]. Most of the developed main-chain-type SPI membranes displayed pretty good proton conductivities. However, the water stability of these SPI membranes could not satisfy the DMFC requirements. Okamoto and his coworkers reported the side-chain-type SPIs bearing pendant sulfoalkoxy groups based on 2,2′-bis(3-sulfopropoxy)benzidine (2,2′-BSPB) and 3,3′-bis(3-sulfopropoxy)benzidine (3,3′-BSPB) [29]. They found that the side-chain-type SPIs exhibited higher proton conductivities than Nafion 117 and better water stability than main-chain-type SPIs. It was confirmed that well micro-phase separated structures played an important role in improving the proton conductivity of the membranes. However, the proton conductivity of the side-chain-type SPIs bearing pendant sulfoalkoxy groups decreased largely at high temperature due to the relatively easy cleavage of sulfopropoxy groups [30]. Aiming at developing proton exchange membranes with good working performance at high temperature, several attempts have been carried out on the investigation of aromatic side-chain-type SPIs [31–34]. The SPIs based on 3,3′- and 2,2′-bis(sulfophenoxy)benzidine (BSPOB) are the typical ones. It has been reported that the BSPOB-based SPI membranes showed high proton conductivities even in low humidity (50% RH) and at high temperature (120 °C). They exhibited good water stability with high mechanical strength and proton conductivity even after aging in water at 130 °C for 500 h. The excellent proton conducting performance of BSPOB-based SPI membranes is considered to be attributed to the thermal stable wholly aromatic structure and the side-chain-type molecular designing.

In this study, a novel side-chain-type sulfonated aromatic diamine, 5-[1,1-bis(4-aminophenyl)-2,2,2-trifluoroethyl]-2-(4-sulfophenoxy) benzenesulfonic acid (BABSA), was synthesized. The sulfonated polyimides bearing sulfonated aromatic pendant groups were prepared from BABSA, NTDA and various non-sulfonated aromatic diamines, *i.e.*, 4,4′-bis(4-amino-2-trifluoromethylphenoxy) biphenyl (6FBAB), 4-bis(4-amino-2-trifluoromethylphenoxy)benzene (6FAPB), and 4,4′-bis(4-aminophenoxy)biphenyl (BAPB), respectively. The SPI membranes are expected to have excellent proton conductivity at high temperature combined with good water stability and low methanol crossover. In order to get the SPI membranes with well micro-phase separated structure, extremely hydrophilic sulfonic acid groups were introduced to the long side chain of the polymer, meanwhile, hydrophobic trifluoromethyl groups were also incorporated to the polymer backbone. It is also known that the trifluoromethyl substituents are effective in improving the oxidation stability and the tensile properties of polyimide membranes [35]. Binaphthyl dianhydride BNTDA with higher electron density in carbonyl carbon atoms was proved to be effective in enhancing the hydrolytic stability of the SPI membranes [36]. Therefore, another series of side-chain-type sulfonated polyimides was also prepared from BNTDA, BABSA and non-sulfonated diamines mentioned above and compared with the NTDA-based SPIs. The solubility and thermal property of the side-chain-type sulfonated polyimides were evaluated. Their mechanical property, water and oxidative stabilities, methanol permeability as well as proton conductivity were investigated. The relationship between the polymer structure and their properties was also discussed.

2. Experimental

2.1. Materials

4-Bromodiphenyl ether and magnesium turnings (Sigma–Aldrich), as well as aniline (Beihua Fine Chemicals Co., China) were used as received. Anhydrous lithium trifluoroacetate was prepared in our laboratory by a reaction of lithium hydroxide and trifluoroacetic acid at 5 °C for 4 h, and then dried under vacuum at 130 °C for 6 h 5-Bromoacenaphthene was prepared via electrophilic substitution of acenaphthene (Sigma–Aldrich) by *N*-bromosuccinimide in *N*,*N*-dimethylformamide (DMF) at room temperature as reported in the literature [37]. Triphenylphosphine (PPh_3) and anhydrous $NiCl_2$ (Beihua Fine Chemicals Co., China) were dried under vacuum. Zinc dust (Acros) was activated in hydrochloric acid under vigorous stirring, then filtrated, washed with diethyl ether and dried under vacuum. 1,4,5,8-Naphthalene tetracarboxylic dianhydride (NTDA) (Beijing Multi Technology Co., China) was purified by vacuum sublimation. 4,4′-Bis(4-amino-2-trifluoromethylphenoxy)biphenyl (6FBAB) and 1,4-bis(4-amino-2-trifluoromethylphenoxy)benzene (6FAPB) (Beijing POME Sci-tech Co., China) were crystallized from ethanol. 4,4′-Bis(4-aminophenoxy)biphenyl (BAPB) (Sigma–Aldrich) was purified by recrystallization from toluene. *m*-Cresol and triethylamine (TEA) was purified by vacuum distillation and dehydrated with 4 Å molecular sieves prior to use. Concentrated sulfuric acid (98%), fuming sulfuric acid (SO_3, 50%), and commercial available solvents, *i.e.*, *N*-methyl-2-pyrrolidone (NMP), *N*,*N*-dimethyl acetamide (DMAc), *N*,*N*-dimethylformamide (DMF) and dimethyl sulfoxide (DMSO) (Beihua Fine Chemicals Co., China), were used as received.

2.2. Monomers synthesis

2.2.1. 4′-Phenoxyl-2,2,2-trifluoroacetophenone (PTFP)

A mixture of anhydrous lithium trifluoroacetate (24.9 g, 0.10 mol), magnesium (2.76 g, 0.115 mol), iodine (0.02 g) and freshly distilled tetrahydrofuran (200 mL) was placed into a 500 mL three-necked round-bottom flask fitted with a dropping funnel, a drying tube, and a reflux condenser. After the anhydrous lithium trifluoroacetate was completely dissolved under stirring, a small part of 4-bromodiphenyl ether (4.9 g, 0.02 mol) was added. The mixture was slowly heated under stirring until the reaction was initiated. Then, the mixture of additional 4-bromodiphenyl ether (20 g, 0.08 mol) and freshly distilled anhydrous tetrahydrofuran (100 mL) was added dropwise. The reaction solution was stirred at room temperature for 4 h, after that, it was slowly heated to 65 °C and kept refluxing for 2 h. The solution was cooled down to room temperature, and then a mixture of concentrated hydrochloric acid (36%, 30 mL) and distilled water (30 mL) was slowly added with agitation. The organic phase was separated, washed with 5% aqueous sodium bicarbonate and distilled with water, dried with anhydrous magnesium sulfate, followed by distilling to remove the solvent. The resulting product was purified by distillation to give colorless liquid of PTFP (19.7 g, 74%). ^{1}H NMR ($CDCl_3$, δ, ppm): 8.04–8.06 (d, 2H); 7.42–7.46 (t, 1H); 7.24–7.27 (d, 2H); 7.09–7.11 (d, 2H); 7.03–7.05 (d, 2H). Elemental analysis: Calculated for $C_{14}H_9F_3O_2$: C, 63.16%; H, 3.41%. Found: C, 63.08%; H, 3.29%.

2.2.2. 1,1-Bis(4′-aminophenyl)-1-(4′′-phenoxyphenyl)-2,2,2-trifluoroethane (BAPTF)

A mixture of PTFP (20 g, 0.075 mol), aniline (75 mL), and aniline hydrochloride (14.5 g, 0.11 mol) was heated to reflux for 24 h. After that, the solution was cooled to room temperature and neutralized with 10% of aqueous sodium bicarbonate. The crude product was obtained by vacuum distillation followed by water vapor distillation to remove excess aniline, which was then purified by recrystallization from ethanol to yield white crystals (24.4 g, 75%). ^{1}H NMR ($CDCl_3$, δ, ppm): 7.32–7.37 (t, 2H); 7.11–7.14 (m, 3H); 7.04–7.07 (d, 2H); 6.89–6.94 (m, 6H); 6.60–6.63 (d, 4H); 3.74 (s, 4H). FTIR (KBr, cm^{-1}): 3454, 3385, 1624, 1587, 1512, 1491, 1286, 1229, 1198, 1150 827, 756,

694. Elemental analysis: Calculated for $C_{26}H_{21}F_3N_2O$: C, 71.88%; H, 4.87%; N, 6.45%. Found: C, 71.68%; H, 4.99%; N, 6.43%.

2.2.3. 5-[1,1-Bis(4′-aminophenyl)-2,2,2-trifluoroethyl]-2-(4″-sulfophenoxy)benzenesulfonic acid (BABSA)

To a 100 mL three-necked flask equipped with a mechanical stirrer, BAPTF (8.68 g, 0.02 mol) was added and cooled with an ice bath. Then concentrated sulfuric acid (8 mL) was slowly added with stirring. After BAPTF was completely dissolved, 3.2 mL of fuming sulfuric acid (SO_3, 50%) was added dropwise. The reaction mixture was stirred at 0 °C for 0.5 h and at 40 °C for 6 h, and then poured into ice water. The resulting white precipitate was collected followed by dissolved in sodium hydroxide solution. The solution was concentrated to give light-brown sodium salt form product BABSA-Na (11.5 g), which was then purified by recrystallization in ethanol aqueous solution. The gained crystal was acidified with concentrated hydrochloric acid. The resulting precipitate was filtered off, washed with water and methanol successively, and dried in vacuo at 120 °C for 10 h to give BABSA (10.82 g, 91%). ^{1}H NMR (BABSA-Na, DMSO-d_6, δ, ppm): 7.74 (s, 1H); 7.54–7.56 (d, 2H); 6.89–6.91 (d, 1H); 6.85–6.87 (d, 2H); 6.73–6.75 (d, 1H); 6.66–6.68 (d, 4H); 6.49–6.51 (d, 4H); 5.16 (s, 4H). FTIR (KBr, cm^{-1}): 3452, 2926, 2624, 1632, 1589, 1514, 1485, 1250, 1196, 1158, 1124, 1094, 1030, 1007, 825, 692, 615, 565. Elemental analysis: Calculated for $C_{26}H_{21}F_3N_2O_7S_2$: C, 52.52%; H, 3.56%; N, 4.71%. Found: C, 71.68%; H, 4.99%; N, 6.43%. Calculated for water content of 6 wt.% in the sample: C, 49.54; H, 3.96; N, 4.45. Found: C, 49.52; H, 4.04; N, 4.41.

2.2.4. Diacenaphthene

A 250 mL three-necked round-bottomed flask equipped with a serum cap, a gas inlet and outlet tube was filled with $NiCl_2$ (0.39 g, 3 mmol), PPh_3 (3.93 g, 15 mmol), zinc dust (11.7 g, 180 mmol) and DMAc (50 mL). The mixture was reacted at 90 °C for 0.5 h under stirring in nitrogen atmosphere. Then a nitrogen purged solution of 5-bromoacenaphthene (10.49 g, 45 mmol) in DMAc (50 mL) was slowly added via a syringe. The mixture was stirred at 90 °C for another 12 h, then concentrated to remove the solvent and poured into 10% of HCl aqueous solution. The dark-gray slurry was separated and dissolved in acetone followed by filtration to remove the insoluble substance. The solution was dried with anhydrous magnesium sulfate and concentrated by evaporation. The yellowish viscous liquid was purified by silica gel column chromatography using hexane as the eluent (3.37 g, 49.7%). ^{1}H NMR ($CDCl_3$, δ, ppm): 7.49–7.51 (d, 2H); 7.39–7.41 (d, 2H); 7.27–7.32 (m, 6H); 3.50 (s, 8H). Elemental analysis: Calculated for $C_{24}H_{18}$: C, 94.08%; H, 5.92%. Found: C, 93.95%; H, 5.89%.

2.2.5. 4,4′-Binaphthyl-1,1′,8,8′-tetracarboxylic dianhydride (BNTDA)

Diacenaphthene (3.06 g, 0.01 mol), sodium dichromate (26.2 g, 0.1 mol), and glacial acetic acid (450 mL) were refluxed at 120 °C for 12 h. After cooling to room temperature, the solution was poured into water (700 mL). The precipitated solid was collected and recrystallized from DMF to give a yellow powder (2.80 g, 71%). m.p. 362 °C. ^{1}H NMR (DMSO-d_6, δ, ppm): 8.70–8.72 (d, 2H); 8.59–8.61 (d, 2H); 7.98–8.00 (d, 2H); 7.79–7.83(t, 2H); 7.73–7.75 (d, 2H). Elemental analysis: Calculated for $C_{24}H_{10}O_6$: C, 73.10%; H, 2.56%. Found: C, 73.04%; H, 2.73%. Mass spectrum (TOF, *m*/*z*, % relative intensity): 394 (M+, 100).

2.3. Polymer synthesis and membrane preparation

2.3.1. Synthesis of sulfonated polyimides

A series of sulfonated copolyimides were prepared via one-step polycondensation from dianhydride NTDA or BNTDA, sulfonated diamine BABSA and non-sulfonated diamine, *i.e.*, 6FBAB, 6FAPB or BAPB, respectively. The molar ratio of sulfonated diamine to non-sulfonated diamine was 3:1. In a typical experiment, SPI-N1, which derived from NTDA, BABSA and 6FBAB, was prepared in the following procedure.

To a completely dried 100 mL three-necked flask equipped with a mechanical stirrer, a nitrogen inlet, and a thermometer, BABSA (1.784 g, 3 mmol), *m*-cresol (20 mL) and TEA (1.2 mL) were fitted. The mixture was stirred at ambient temperature under nitrogen flow until BABSA was completely dissolved to give a homogeneous solution. Then 6FBAB (0.504 g, 1 mmol), NTDA (1.072 g, 4 mmol) and benzoic acid (0.95 g, 7.8 mmol) were added to the solution. The mixture was stirred at room temperature for a few minutes and then heated to 80 °C for 4 h and 180 °C for 20 h, respectively. After the solution was cooled to 80–100 °C, 20 mL of additional *m*-cresol was added to dilute the highly viscous solution. The fiber-like precipitate was obtained as the solution was poured into acetone, and then collected by filtration, washed with acetone, and dried in vacuum at 120 °C for 12 h.

The other sulfonated polyimides, *i.e.*, SPI-N2 (NTDA/BABSA/6FAPB), SPI-N3 (NTDA/BABSA/BAPB), SPI-B1 (BNTDA/BABSA/6FBAB), SPI-B2 (BNTDA/BABSA/6FAPB) and SPI-B3 (BNTDA/BABSA/BAPB) were synthesized by the similar procedure, except that different kinds of dianhydrides and non-sulfonated diamines were applied.

2.3.2. Membrane preparation

Membranes of the sulfonated polyimides were prepared by casting the *m*-cresol solutions of polymers in TEA salt form (7–10 wt.%) on glass plates and drying at 120 °C for 10 h. The as-cast membranes were soaked in methanol at 60 °C for 4–5 h to remove the residual solvent followed by proton-exchange treatment in 1 mol/L HCl at room temperature for 10–12 h. The proton-exchanged membranes were thoroughly washed with water and then dried in vacuo at 150 °C for 10 h. The membrane thickness was 50–60 μm.

2.4. Characterization

2.4.1. Measurements

^{1}H NMR and ^{13}C NMR spectra were performed on a Bruker Avance 400 spectrometer operating at 400 MHz in $CDCl_3$ and DMSO-d_6. FTIR spectra were recorded on a Perkin–Elmer 782 Fourier transform spectrophotometer. Mechanical properties were measured on an Instron 3365 Tensile Apparatus with 80 × 10 × 0.05 mm specimens at 25 °C and about 40% RH at a crosshead speed of 2 mm/min. Differential scanning calorimetry (DSC) was carried out using a TA Q100 instrument in nitrogen at a heating rate of 10 °C/min. Thermal gravimetric analysis (TGA) was performed on a TA Q50 instrument in nitrogen at a heating rate of 20 °C/min. Transmission electron microscopy (TEM) photographs were taken on a JEM-1011 transmission electron microscope, using an accelerating voltage of 100 kV. In order to stain the ionic domains, membrane samples in proton form were converted into Ag^+ form by immersing them in 0.5 M $AgNO_3$ aqueous solution overnight and then thoroughly rinsed with water, dried at room temperature for 12 h before measurement.

2.4.2. Ion exchange capacity (IEC) and water uptake, dimensional change

The ion exchange capacity (IEC) was evaluated by means of titration. The dried SPI membranes were soaked in 15 wt.% NaCl solution at 30 °C for 48 h, then the protons released due to the exchange reaction with Na^+ ions were titrated with a 0.02 M NaOH solution using phenolphthalein as an indicator. IEC value was calculated from:

$IEC = (V \times N_{NaOH})/W$
where V is the volume of NaOH consumed, N_{NaOH} is the normality of NaOH solution, and W is the weight of sample.

Water uptake was also measured by immersing the SPI membranes into water at 30 °C for 24 h. Then the membrane was taken out, quickly wiped with a tissue paper and weighed on a microbalance. Water uptake (WU) was calculated from:

$WU = (W_s - W_d)/W_d \times 100$ wt.%
where W_s and W_d are the weights of hydrated and dried membranes, respectively.

Dimensional change of SPI membranes was measured by immersing the round-shaped samples (Ø40 × 0.05 mm) in water at 25 °C for 4–5 h. The changes of thickness (Δt_c) and diameter (Δl_c) were calculated from:

$\Delta t_c = (t - t_s)/t_s$ and $\Delta l_c = (l - l_s)/l_s$
where t_s and l_s are the thickness and diameter of membranes equilibrated at 25 °C and 70% RH for 24 h, respectively; t and l refer to those of the membranes immersed in water for 4–5 h.

2.4.3. Water stability and oxidative stability

The water stability was carried out by immersing SPI membranes into distilled water at 100 °C and the stability was evaluated by the elapsed time for the samples start to lose their mechanical strength.

The oxidative stability of SPI membranes was determined by immersing the samples (10 × 10 × 0.05 mm) into Fenton's reagent (30 ppm $FeSO_4$ in 30% H_2O_2) at 30 °C, which was evaluated by recording the time when the samples began to dissolve and dissolved completely.

2.4.4. Proton conductivity

Proton conductivity in plane direction of SPI membrane was determined using a four-point-probe electrochemical impedance spectroscopy technique over the frequency from 10 Hz to 100 KHz (Hioki 3522-50). A membrane sample (40 × 10 × 0.05 mm) and two pieces of platinum plate electrodes were set in a Teflon cell. The distance between the two electrodes was 2 cm. The cell was placed in distilled water for measurement at 100% RH. The resistance value associated with the membrane conductance was determined from high frequency intercept of the impedance with the real axis. Proton conductivity (σ) was calculated from:

$\sigma = d/(t_s \cdot w_s \cdot R)$
where d is the distance between the two electrodes, t_s and w_s are the thickness and width of the membrane, and R is the resistance value measured.

2.4.5. Methanol permeability

Methanol permeability of membrane was measured using a liquid permeation cell composed of two compartments, which were separated by a vertical membrane. One compartment of the cell (A) was filled with methanol aqueous solution (C_A = 30 or 50 wt.%), the other compartment (B) was filled with distilled water. The tested membrane was immersed in water to get swollen sample and then set into the measurement cell. The solutions in both compartments were kept at 30 °C and stirred continuously during the permeation measurement. The methanol concentration of compartment B (C_B) was analyzed by a gas chromatograph (Shimadzu, GC-2014). The methanol permeability (P_M) was calculated by the following equation:

$P_M = (k \cdot V_B \cdot L)/(A \cdot C_A)$

where k is the slope of the straight-line plot of C_B versus permeation time, V_B is the volume of solution B, L and A are the thickness and effective area of the tested membrane.

3. Results and discussion

3.1. Monomers synthesis

The side-chain-type sulfonated diamine BABSA was synthesized by a three-step reaction process as shown in Scheme 1. First, PTFP was prepared by the Grignard reaction between anhydrous lithium trifluoroacetate and 4-bromodiphenyl ether in the presence of magnesium in THF. Then, the diamine BAPTF was synthesized by the coupling of 1 equiv of PTFP with 2 equiv of aniline catalyzed by aniline hydrochloride at about 185 °C. After that, BAPTF was sulfonated with fuming sulfuric acid (50% SO_3) and precipitated as the inner salt, which was then neutralized with sodium hydroxide solution to get sodium salt form intermediate BABSA-Na. Finally, the sulfonated diamine BABSA was obtained by acidification of BABSA-Na with hydrochloric acid.

Fig. 1 shows the ^{1}H NMR spectra of compounds PTFP and BAPTF, in which all the protons in the structure could be assigned easily according to the integral values of the intensity. In addition, the elemental analysis values for PTFP and BAPTF were also in good agreement with the calculated ones. The ^{1}H NMR and ^{13}C NMR spectra of sodium form intermediate BABSA-Na is shown in Fig. 2. In the ^{1}H NMR spectrum, the signal assigned to the protons in amino groups was observed at 5.16 ppm. The aromatic protons H_1–H_5 showed the doublet peaks at 6.49–6.91 ppm. The aromatic protons adjacent to the $-SO_3Na$ groups (H_6 and H_7) shifted to the downfield because of the strong electron-withdrawing effect of the $-SO_3Na$ groups, which were observed at 7.54–7.56 and 7.74 ppm, respectively. In the ^{13}C NMR spectrum, the carbon in trifluoromethyl group (C_6) showed the clear quartet absorption at 124–133 ppm because of the coupling interaction of the carbon atom with fluorine atoms in the diamine molecule. All of other carbon atoms could be clearly assigned as expected.

The structure of BAPTF and BABSA were further confirmed by means of FTIR spectra. As shown in Fig. 3, the characteristic absorptions around 3450 cm^{-1} and 1151 cm^{-1}, which due to the

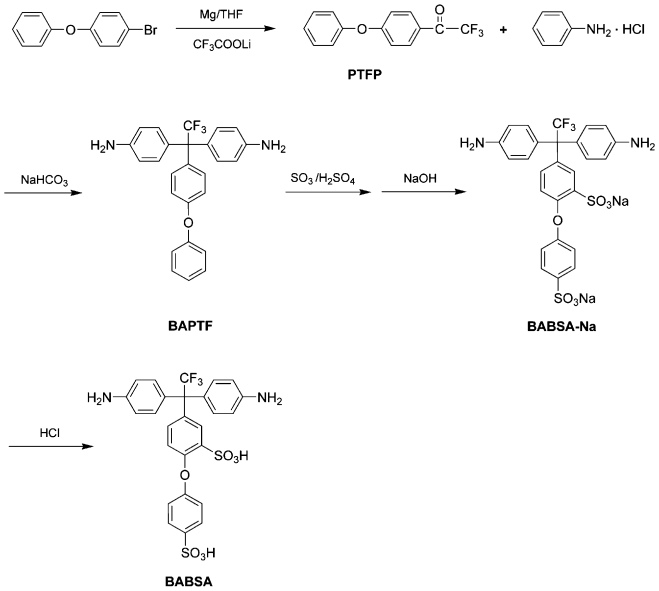

Scheme 1. Synthesis of side-chain-type sulfonated aromatic diamine BABSA.

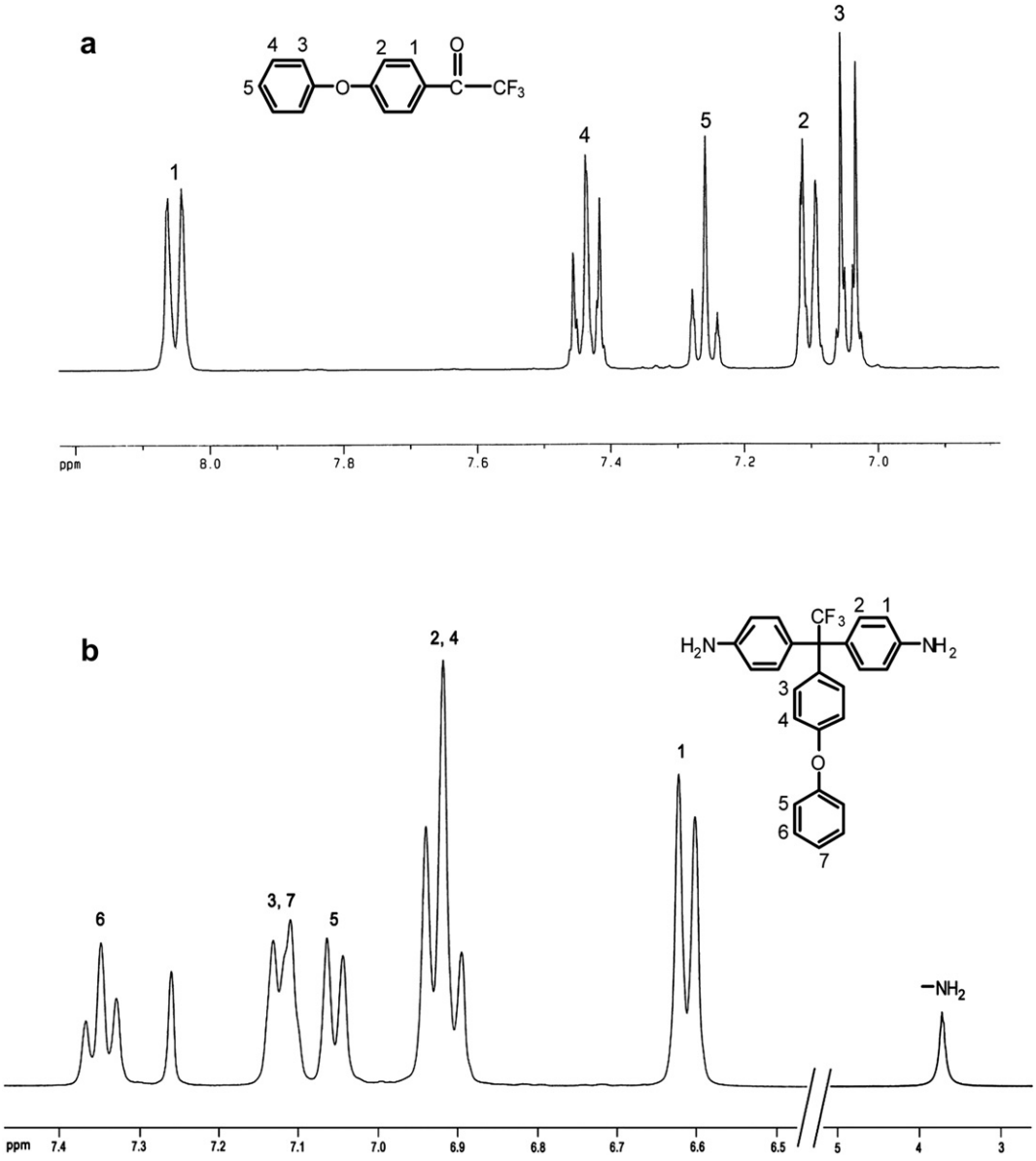

Fig. 1. ^{1}H NMR spectra of PTFP (a) and BAPTF (b) in $CDCl_3$.

N–H stretching vibration of amino groups and the C–F stretching vibration of trifluoromethyl group, respectively, were detected for both of BAPTF and BABSA. In addition, the broad absorption band around 1250 cm^{-1} and the absorption at 1030 cm^{-1}, which assigned to the stretching vibration of sulfonic acid groups, were also observed in the FTIR spectrum of BABSA. The elementary analysis result for BAPTF was in good agreement with the calculated one. However, the found value of elementary analysis for BABSA was slightly different from the calculated value. This is mainly caused by the adsorbed water in the BABSA sample (*ca.* 6 wt. %). The characterization results indicated that the obtained sulfonated diamine BABSA was pure enough to be employed for preparation of polyimides.

The synthesis of BNTDA via a four-step reaction process had been reported by several groups [38,39], in which 4-chloro-1,8-naphthalix anhydride was firstly converted into ester followed by coupling to afford the tetraester and subsequent hydrolysis and dehydration to provide the dianhydride BNTDA. In this study, the dianhydride BNTDA was prepared via a two-step reaction route as shown in Scheme 2. The diacenaphthene was firstly synthesized by coupling of 5-bromoacenaphthene catalyzed by Ni(0) at 90 °C, which was then oxidized by sodium dichromate in glacial acetic acid to afford BNTDA. The reaction process is very simple and the reaction condition is moderate as comparing with that reported. The chemical structure of BNTDA was clearly identified by means of ^{1}H NMR spectroscopy. The elemental analysis values were in good agreement with the calculated ones, which also provided clear confirmation of the structure and the purity of the product. The dinaphthalic dianhydride BNTDA is yellow powder and stable to the moisture in air at room temperature.

3.2. Polymer synthesis and characterization

A series of sulfonated copolyimides were synthesized by a one-step method from dianhydrides NTDA or BNTDA, sulfonated diamine BABSA and various non-sulfonated diamines, respectively,

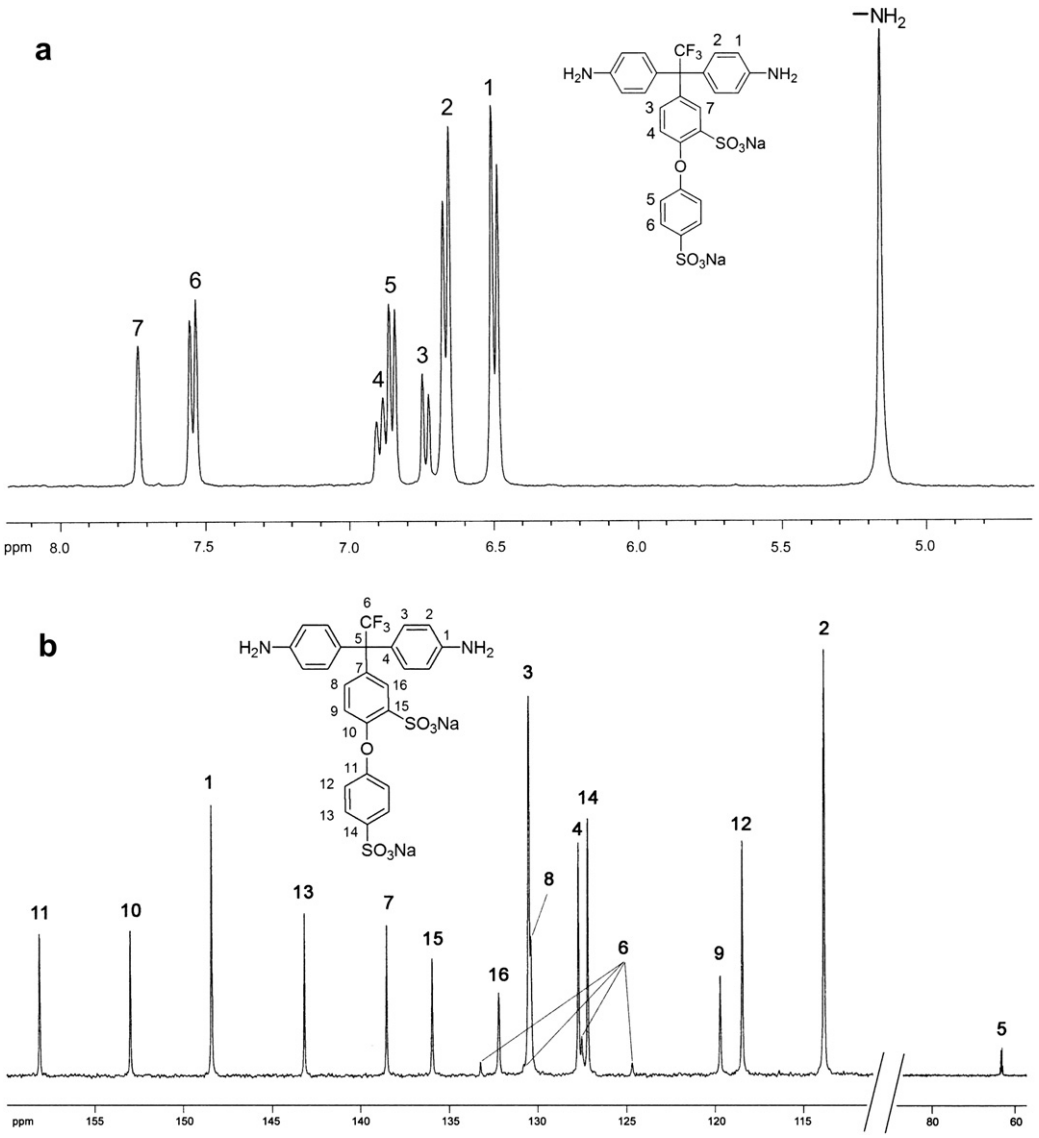

Fig. 2. ^{1}H NMR (a) and ^{13}C NMR (b) spectra of BABSA-Na.

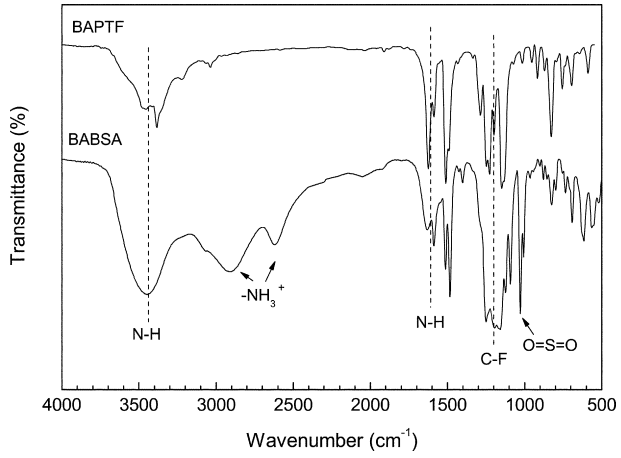

Fig. 3. FTIR spectra of BAPTF and BABSA.

in *m*-cresol with the presence of TEA and benzoic acid as illustrated in Scheme 3. TEA was used to liberate the protonated amino groups for polymerization with dianhydrides and benzoic acid acted as a catalyst. This method has been employed for preparation of many other sulfonated polyimides in the literature [40]. The molar ratio of sulfonated diamine BABSA to non-sulfonated diamine was 3:1, which give a fixed sulfonation degree of 75%. Fiber-like precipitates could be gained as the polymer solution was poured into acetone, indicating that the polymers have relatively high molecular weight.

Fig. 4 shows the FTIR spectra of the SPI membranes. For the SPI-N membranes derived from dianhydride NTDA, the characteristic absorptions of naphthalenic imide rings were observed at 1715 cm^{-1} (C═O, symmetric), 1676 cm^{-1} (C═O, asymmetric) and

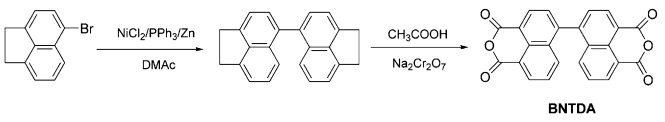

Scheme 2. Synthesis of dianhydride BNTDA.

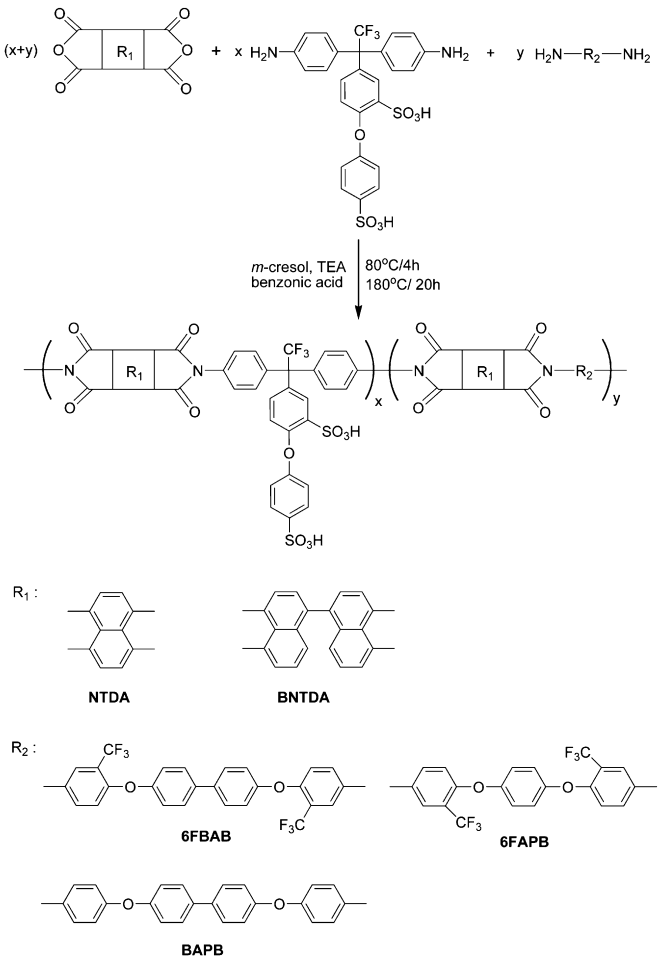

Scheme 3. Synthesis of sulfonated polyimides.

1350 cm^{-1} (C–N, asymmetric), respectively, which were lower than those for the phthalimide (*e.g.*, 1780, 1720 and 1375 cm^{-1}). The absorption assigned to the stretching vibrations of sulfonic acid groups were found at 1094 and 1026 cm^{-1}. For the SPI-B membranes derived from dianhydride BNTDA, it was found that the absorption bands of C=O stretching vibration shifted down to 1710 and 1670 cm^{-1}, while the absorption band of C–N stretching vibration shifted up to 1365 cm^{-1}, respectively. The characteristic absorption bands for sulfonic acid groups showed no significant difference from that for SPI-N membranes. Moreover, for the SPI membranes prepared from non-sulfonated diamines 6FBAB and 6FAPB, *i.e.*, SPI-N1, SPI-N2, SPI-B1 and SPI-B2, the absorption attributed to the C–F stretching vibration of trifluoromethyl group was detected at 1054 cm^{-1}. The ^{1}H NMR spectra of SPI-N3 and SPI-B3 are shown in Fig. 5. All of the protons could be well assigned to the expected polymer structure and the integration intensity ratio of diamine moieties protons over naphthalenic or dinaphthalenic protons was found in good accordance with the theoretical ones, indicating the complete polycondensation.

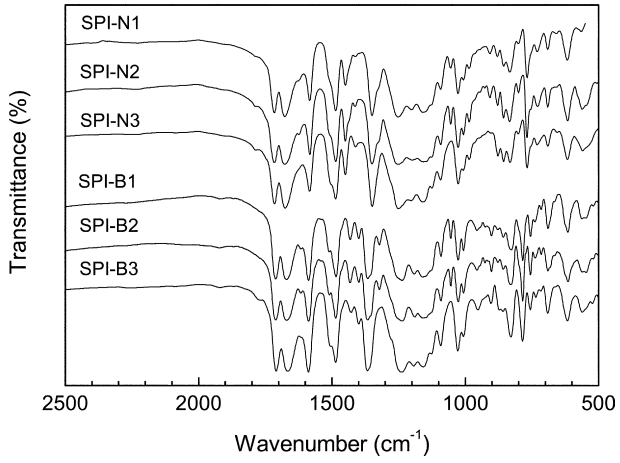

Fig. 4. FTIR spectra of SPI membranes.

The solubility of sulfonated polyimides in TEA salt form and in proton form was determined by dissolving the polymer resins in different organic solvents with 5 wt.% of solid content followed by stirring for 24 h. As shown in Table 1, the SPIs displayed better solubility in the TEA salt form than that in the proton form. All the SPIs in TEA salt form could be completely dissolved in the chosen solvents. The SPIs in proton form also could be easily dissolved in the testing solvents except in *m*-cresol. The SPI-N1, SPI-N2, SPI-B2 and SPI-B3 in proton form were partially soluble in *m*-cresol at room temperature, whereas, they could be dissolved after heating at 50 °C. The solubility was mainly governed by the structure of the sulfonated diamine moieties. The good solubility of the present SPIs was due to the synergetic effects of the bulky aromatic pendant groups and the fluorine groups in the backbones, which disrupted the regularity of the molecular chains and hindered the dense chain stacking, thus increased the solubility. The polymer solutions were very stable and no phase separation or precipitation was observed after storage for several weeks.

3.3. Mechanical and physical properties

All the synthesized SPIs displayed pretty good film forming abilities. Tough, flexible and transparent membranes could be obtained by casting the *m*-cresol solutions of SPIs in TEA salt form onto glass plates followed by thermal baking to remove the solvent and subsequent proton-exchange treatment and drying. The mechanical properties of the dry SPI membranes are listed in Table 2. All the membranes exhibited good tensile strength and fracture toughness. Both of SPI-N and SPI-B membranes displayed higher Young's modulus and tensile strength than Nafion 115, suggesting better mechanical properties of them. As comparing the mechanical properties of SPI-N with that of SPI-B membranes, it is found that the former gave the tensile strengths of 69.5–74.6 MPa, which were 17.2–22.8 MPa higher than those of the latter with same diamine moieties. This indicates that the SPI-N membranes were stiffer than the SPI-B membranes. The elongation at break of SPI-N membranes was around 10% and that for SPI-B membranes was in the range of 6.8–10.6%. Considering the membranes were completely dried before measurement, the flexibility of the SPI membranes was pretty good. If the membranes were partially or fully hydrated, the flexibility must be greatly improved.

Ion exchange capacity (IEC), water uptake and the number of water molecules per sulfonic acid group (λ) of SPI membranes are summarized in Table 3. The IEC values measured by titration were in good agreement with the theoretical ones. Although these membranes were designed with fixed sulfonation degree of 75%, the SPI-N membranes gave the theoretical IEC values of 1.87–1.95 meq/g, which were much higher than that of SPI-B membranes (1.61–1.67 meq/g). This is related with the difference in molecular weight of NTDA and BNTDA.

It is well known that the water uptake mainly depends on the IEC of the membrane.[34] For SPI membranes, higher IEC value usually leads to the larger water uptake. As expected, the water

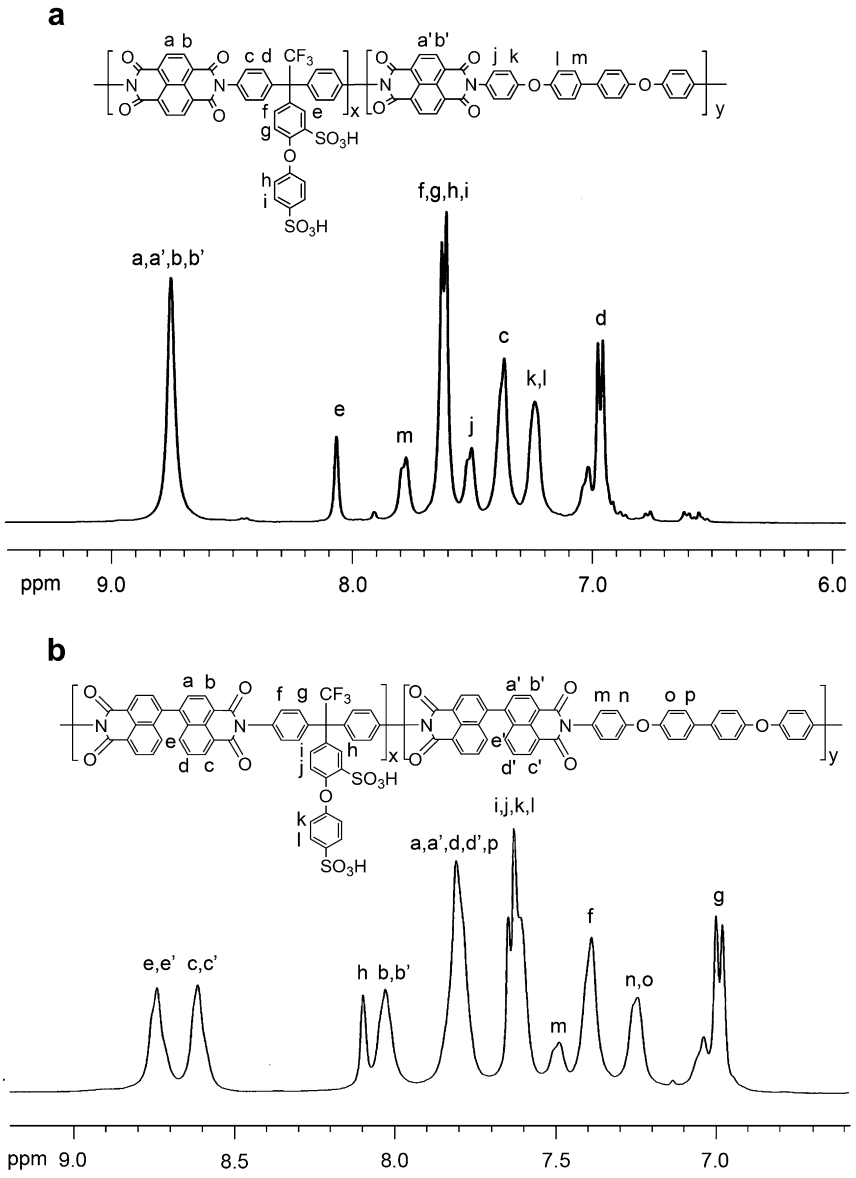

Fig. 5. ^{1}H NMR spectra of (a) SPI-N3 and (b) SPI-B3 in DMSO-d_6.

uptakes of SPI-N membranes were much higher than that of SPI-B membranes. The water uptake is also affected by the polymer structure to a certain extent. As comparing the SPI membranes, which have different molecular structures, it is also found that SPI-N1 and SPI-N2, which have higher fluorine content than SPI-N3 but no significant difference in IEC values, exhibited lower water uptakes. This could be explained by the existence of hydrophobic CF_3 groups in the polymer backbone, which resulted in the reduction of water adsorption. However, the SPI-B1 and SPI-B2 showed the water uptakes similar to SPI-B3, although the former have higher fluorine content. We suspect that it is related to the twisted noncoplanar naphthalene structure in polymer backbone,

Table 1
Solubility of sulfonated polyimides in TEA salt form and in proton form.[a]

SPIs	Form	*m*-Cresol	NMP	DMAc	DMF	DMSO
SPI-N1	TEA^+	++	++	++	++	++
	H^+	+	++	++	++	++
SPI-N2	TEA^+	++	++	++	++	++
	H^+	+	++	++	++	++
SPI-N3	TEA^+	++	++	++	++	++
	H^+	++	++	++	++	++
SPI-B1	TEA^+	++	++	++	++	++
	H^+	++	++	++	++	++
SPI-B2	TEA^+	++	++	++	++	++
	H^+	+	++	++	++	++
SPI-B3	TEA^+	++	++	++	++	++
	H^+	+	++	++	++	++

[a] ++: Soluble; +: Partially soluble.

Table 2
Mechanical properties of SPI membranes.

Membranes	Young's Modulus (GPa)	Tensile Strength (MPa)	Elongation at Break (%)
SPI-N1	1.85	72.7	10.3
SPI-N2	2.06	74.6	9.5
SPI-N3	1.89	69.5	9.7
SPI-B1	1.97	55.0	8.5
SPI-B2	1.76	51.8	10.6
SPI-B3	1.94	50.0	6.8
Nafion 115	0.25	43.0	225

Table 3
Physical properties of SPI membranes.

Membranes	IEC (meq/g)		F Content (wt.%)	Wu (wt.%)	λ	Dimensional Change	
	Calculated	Measured				Δt_c	Δl_c
SPI-N1	1.87	1.81	8.86	62.4	19	0.12	0.15
SPI-N2	1.91	1.86	9.07	67.8	20	0.18	0.15
SPI-N3	1.95	1.88	5.55	73.7	22	0.22	0.17
SPI-B1	1.61	1.57	7.66	42.6	15	0.09	0.09
SPI-B2	1.65	1.61	7.82	48.5	17	0.07	0.11
SPI-B3	1.67	1.60	4.77	45.5	16	0.13	0.11
SPI-B3′	1.89	1.82	5.39	78.4	24	0.16	0.17
Nafion115	0.91	–	–	24.0	15	0.16	0.08

which induced the decrease of the interaction of polymer chain and the increase of inter-chain spacing. Therefore, there were more water molecules occupied in the inter-chain spacing and adsorbed to the sulfonic acid groups [41]. We have also prepared SPI-B3′ membrane with similar structure to SPN-B3 except the sulfonation degree increased to 87.5%. We noticed that the water uptake of SPI-B3′ (78.4%) was higher than that of SPI-N, although they have close IEC values. It is also demonstrated that more water molecules adsorbed to per sulfonic acid group in the SPI-B membranes.

The number of water molecule per acid group (λ) was determined from water uptake and measured IEC value by equation $\lambda = n(H_2O)/n(SO_3^-) = WU/18 \cdot IEC$. It is found that SPI-N membranes showed very similar λ values of 19–22, which were much higher than that of Nafion 115 ($\lambda = 15$). It is suggested that more water molecules adsorbed to per sulfonic acid groups. The SPI-B membranes also exhibited close λ values of 15–17, which were lower than SPI-N membranes because of their relatively low IEC. But the λ values of SPI-B were still comparable to Nafion 115.

The dimensional changes of the membranes equilibrated in water at 30 °C were evaluated and the results are listed in Table 3. In general, most of the SPI membranes reported in the literature exhibit anisotropic swelling in water [42], which is similar to the swelling behavior observed for Nafion 115. However, both of SPI-N and SPI-B membranes showed isotropic membrane swelling in water because of the rigid aromatic pendant groups in the polymer structure. It is considered that the large (or long) rigid aromatic pendant groups make the orientation of polymer chains in plane direction difficult, resulting in rather random orientation of polymer chains [33]. Moreover, the SPI-B membranes displayed better dimensional stability than SPI-N membranes with changes in thickness and in plane direction no more than 13%, which is related to the low water uptakes of SPI-B.

3.4. Membrane stabilities

The water stability of membranes is one of the most important factors affecting the membrane performance. It is considered that water stability of membranes is affected by the chemical structure, configuration and the basicity of sulfonated diamine [43]. As shown in Table 4, all the SPI-N and SPI-B membranes displayed reasonably good water stability. The membranes could keep their original shape until soaking in boiling water for 191–500 h. The good water stability is related to the side-chain-type structure of sulfonated diamine BABSA. The long side chain with extremely hydrophilic sulfonic acid groups could make the water molecules mainly gathering around the lateral chains and protect the main-chain imide rings from hydrolysis. Moreover, the sulfonated diamine BABSA displayed relatively high basicity because the sulfonic acid groups appending in the side chains were separated from the amine groups. The high basicity of the sulfonated diamine lowered the positive electricity of carbonyl groups in imide rings, and therefore, the hydrolytic reaction was depressed [44]. The SPI-B membranes displayed much better water stability than SPI-N membranes. This is not only due to their low IEC level but also related to the introduction of BNTDA. It is known that electron density of the carboxyl carbon atoms in BNTDA-based SPI was much higher than that of NTDA-based SPI because of the lower electron affinity of BNTDA, which restrained the nucleophilic attack of the water molecules on the carboxyl groups. A similar result was also reported by Ding et al. as they investigated the other BNTDA-based sulfonated polyimides [36]. Furthermore, it is noted that SPI-B2 membrane exhibited the best water stability, which did not break into pieces until the membrane soaking in boiling water for 500 h. This can be explained by the flexible main chain of SPI. The non-sulfonated diamine 6FAPB is more flexible than 6FBAB and BAPB due to the three phenyl rings linked with ether bonds, which providing much more flexible main chain for SPI-B2. It has been reported that a flexible chain can undergo relaxation more easily than the rigid ones [25]. Therefore, SPI-B2 displayed better water stability than the others.

Membrane stability towards oxidation was examined by observing the dissolving behavior in Fenton's reagent at 30 °C. The oxidation stability of the membranes was characterized by elapsed time that the membrane started to dissolve in the solution (τ_1) and dissolved completely in the solution (τ_2). As shown in Table 4, all SPI-N and SPI-B membranes displayed fairly good stability to oxidation due to the wholly aromatic sulfonated diamine. The elapsed time of the membranes started to dissolve and dissolved completely in the solution were in the ranges of 21–48 h and 36–76 h, respectively. It is also found that SPI-N membranes showed better stability to oxidation than the corresponding BNTDA-based membranes. This can be interpreted by the relatively high content of hydrophobic trifluoromethlyl groups, which could protect the polymer main chain from being attacked by water molecules containing highly oxidizing radical species [45]. It is known that the fluorinated substituents in the polymer backbone are effective in the improvement of oxidation stability of sulfonated polyimide. However, we noted that the SPI-N1 and SPI-B1, both of

Table 4
The water stability, oxidative stability and thermal stability of SPI membranes.

Membranes	Water Stability (h)	Oxidative Stability[a]		Thermal Stability[b]	
		τ_1 (h)	τ_2 (h)	T_{d1} (°C)	T_{d2} (°C)
SPI-N1	191	47	76	299.1	551.8
SPI-N2	237	37	47	305.0	553.8
SPI-N3	290	29	49	329.2	553.9
SPI-B1	264	48	61	283.9	554.3
SPI-B2	501	24	36	286.4	559.6
SPI-B3	468	21	44	300.7	560.2

[a] τ_1 and τ_2 refer to the elapsed time that the membranes began to dissolve and dissolved in the solution, respectively.
[b] T_{d1} and T_{d2} refer to the decomposition temperature of sulfonic acid group and the decomposition temperature of polymer backbone, respectively.

which derived from non-sulfonated diamine 6FBAB, displayed much better durability in Fenton's regent with longer time of the membranes started to dissolve than the others, despite their fluorine contents were not as high as SPI-N2. This may be related with the combined effects of high fluorine content and rigid biphenyl structure of 6FBAB in the polymer backbone.

The thermal stability of SPIs was evaluated by TGA measurement. As shown in Fig. 6, all the membranes exhibited three-step weight loss. The first weight loss below 150 °C is due to the evaporation of water absorbed in the polymers; the second one in the range of 280–330 °C is attributed to the thermal decomposition of sulfonic acid groups; the third one up to 550 °C is assigned to the degradation of polymer main chain. The thermal stability of SPIs mainly depends on the cleavage temperature of sulfonic acid groups. The SPI-N membranes showed better heat resistance as comparing with the corresponding SPI-B membranes with the desulfonation temperature of 299–329 °C, which was much higher than the common main-chain-type sulfonated polyimides and some side-chain-type ones [46].

3.5. Proton conductivity

Proton conductivity is the most important factor that affects the performance of a fuel cell system. In this study, the proton conductivity of the SPI membranes was measured in the temperature range of 30–80 °C at 100 RH%. For comparison, the proton conductivity of Nafion 115 was also determined at the same conditions. Fig. 7 shows the temperature dependence of proton conductivity for SPI-N, SPI-B and Nafion 115 membranes. The proton conductivities (σ) measured at 30 °C for these membranes are summarized in Table 5.

The σ values of all the membranes increased with the temperature rising. The proton conductivities of SPI-N membranes in water at 30 °C were in the range of 0.086–0.095 S/cm, which is comparable to that of Nafion 115 (0.095 S/cm). It is noteworthy that the SPI-N membranes exhibited better proton conductivity than Nafion 115 as the temperature over 40 °C. The proton conductivities for SPI-N measured at 80 °C increased to 0.18–0.22 S/cm, while that for Nafion 115 was 0.15 S/cm. The high conducting performance of SPI-N membranes can be explained from the view of activation energy of proton conductivity. The proton conductivity of membranes showed an Arrhenius-type temperature dependence. The activation energies of proton conductivity (ΔE_{aC}) for SPI-N membranes were 11–17 kJ/mol, while the value for Nafion 115 was 8 kJ/mol. The SPI-N membranes showed higher activation energies

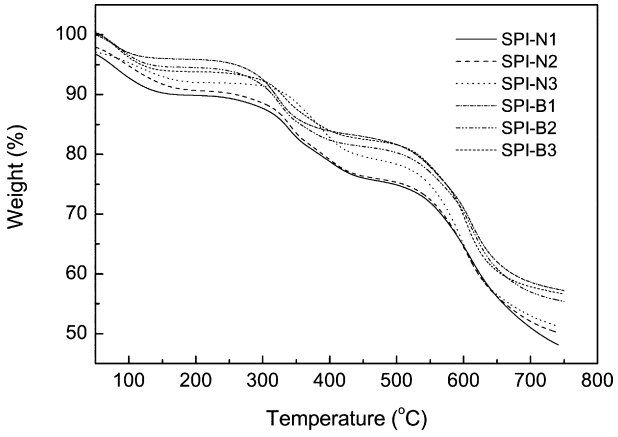

Fig. 6. TGA curves of SPI membranes (in nitrogen).

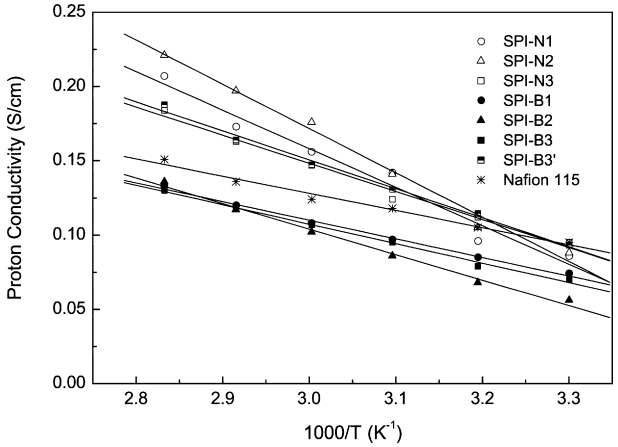

Fig. 7. Temperature dependence of proton conductivity for SPI and Nafion 115 membranes at RH 100%.

than Nafion 115, therefore, the σ values for the former increased faster than that for Nafion 115 with the temperature rising.

The proton conductivities for SPI-B membranes in water at 30 °C were relatively lower than that for SPI-N and Nafion 115 membranes with the σ values of 0.056–0.074 S/cm. Although the SPI-B membranes showed lower σ values than Nafion 115 in the tested temperature range, the difference in proton conductivity between them gradually decreased with the temperature increasing owing to their relatively higher activation energies (10–16 kJ/mol). The proton conductivities of SPI-B membranes at 80 °C were close to that of Nafion 115 with the σ values of 0.13–0.14 S/cm. The low conducting performance of SPI-B membranes is associated with their lower IEC values. We have investigated the proton conductivity of the above mentioned SPI-B3′ membrane, whose IEC value was close to SPI-N membranes. It is found that the SPI-B3′ membrane gave the σ value of 0.093 S/cm at 30 °C and showed a similar increasing tendency with SPI-N3 in the tested temperature range.

3.6. Methanol permeability

Methanol permeability is a key parameter for membranes using in DMFC. To achieve high fuel cell performance, membranes should have not only high proton conductivity but also low methanol permeability. The methanol permeability (P_M) measured at 30 °C with different methanol content in feed and the ratios (Φ) of proton conductivity to methanol permeability of SPI and Nafion 115 membranes are summarized in Table 5.

All the SPI membranes showed much lower methanol permeability than Nafion 115. The P_M values for SPI-N and SPI-B membranes tested at 30 °C with 30 wt.% of methanol content in feed, decreased to 50% and 25% of that for Nafion 115. With an

Table 5
Proton conductivity, methanol permeability and the ratio of proton conductivity to methanol permeability of SPI and Nafion 115 membranes.

Membranes	σ (S/cm)	P_M (10^{-6} cm^2/s)		Φ (10^4 S cm^{-3} s)	
		30%	50%	30%	50%
SPI-N1	0.086	0.81	0.95	10.6	9.1
SPI-N2	0.088	0.74	0.98	11.9	9.0
SPI-N3	0.095	0.74	0.76	12.8	12.5
SPI-B1	0.074	0.40	0.50	18.5	14.8
SPI-B2	0.056	0.45	0.45	12.4	12.5
SPI-B3	0.070	0.47	0.46	15.0	15.3
Nafion115	0.095	1.58	1.91	6.0	5.0

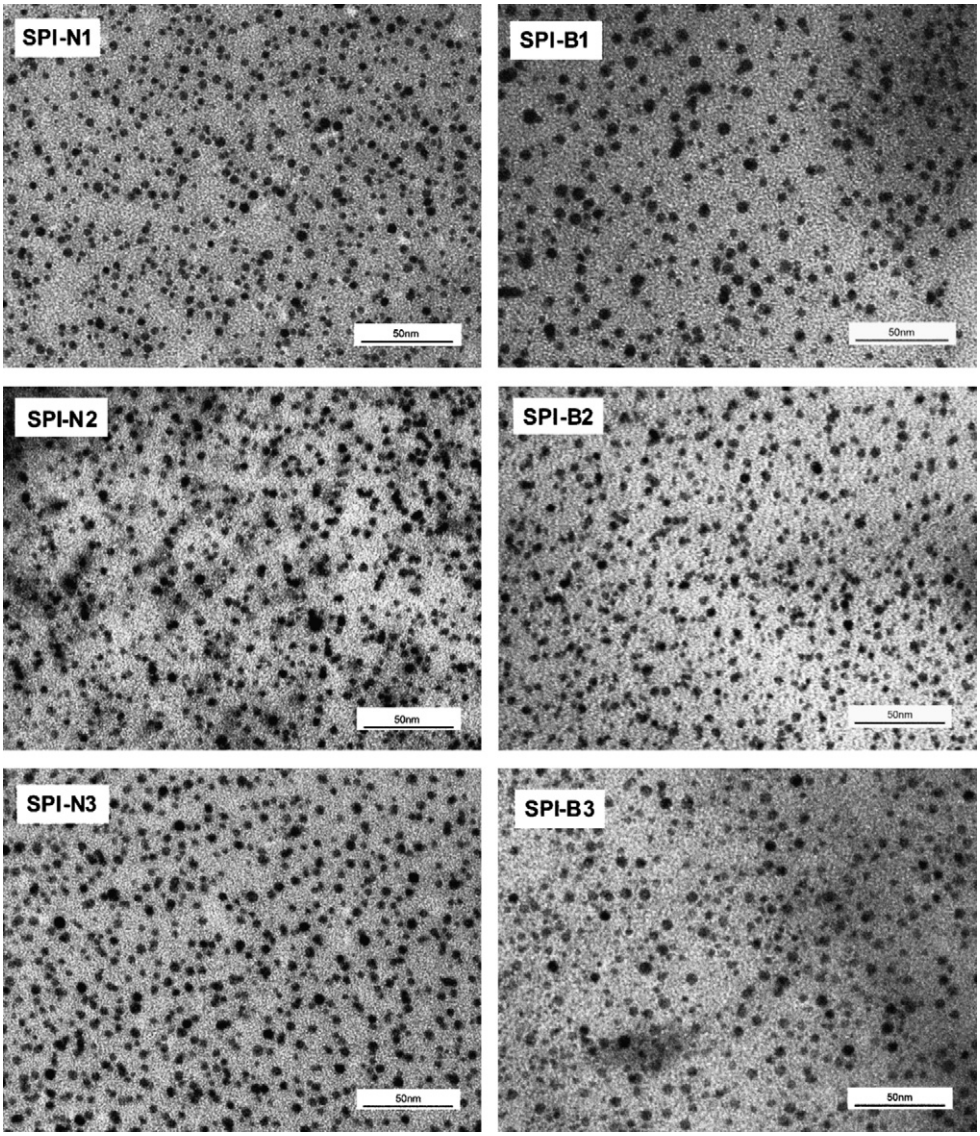

Fig. 8. TEM micrographs of SPI membranes (cross section, in Ag^+ form).

increase in methanol content in feed from 30 wt.% up to 50 wt.%, the P_M values for Nafion 115 increased from 1.58×10^{-6} cm^2/s to 1.91×10^{-6} cm^2/s. On the other hand, the P_M values for SPI-N and SPI-B membranes showed hardly dependence on the methanol content in feed, which slightly increased for the former and kept almost same for the latter. As comparing the P_M values of SPI membranes with different structures, it is found that SPI-B displayed lower methanol permeability than SPI-N. The difference in methanol permeability between the SPI membranes can be explained by the dissimilarity in their microstructure. It is known that methanol mainly permeates through the hydrophilic domains consisting of sulfonic acid groups. The Nafion membranes is known to have well-developed hydrophobic/hydrophilic microphase separation structure. The well connected hydrophilic domains provide not only proton conducting channel but also methanol permeating pathways. However, the hydrophobic/hydrophilic microstructure in SPI membranes is less separated due to their rigid and less hydrophobic backbone as well as the less acidic sulfonated functional groups. Therefore, the narrower transport channels in SPI membranes result in the lower methanol permeability compared with Nafion membranes.

It is also found that the SPI-N1 and SPI-N2 membranes, which derived from fluorine-containing non-sulfonated diamines 6FBAB and 6FAPB, respectively, gave higher P_M values and displayed certain dependence on the concentration of methanol in feed than the other SPI membranes. This is considered to be related to their better hydrophobic/hydrophilic microphase separation structure because of the presence of hydrophobic trifluoromethyl groups in the polymer backbone. The good hydrophobic/hydrophilic microstructure played a promoting role in not only proton but also methanol transport in membranes. The microstructures of SPI membranes will be discussed below in more details.

The ratio Φ, which calculated from σ to P_M, is an effective parameter evaluating the membranes performance in a DMFC system. All the SPI membranes displayed fairly high Φ values ranging from 10.6×10^4 S cm^{-3} s to 18.5×10^4 S cm^{-3} s as calculated from the P_M values with 30 wt.% of methanol content in feed. Their Φ values were almost two to three times of the Nafion 115. Moreover, the SPI-B membranes gave the higher Φ values than SPI-N membranes. There is no significant dependence of Φ values on the methanol concentration in feed were observed for all the membranes. The good permselectivity of SPI membranes is

attributed to their much smaller methanol permeabilities as compared with Nafion 115.

3.7. Membrane morphology

It is considered that there is a close contact between the microphase separation structure and the proton conductivity of the membranes. In order to get a comprehensive understanding of the proton conductivity behavior of membranes, we tried to investigate the microstructure of the SPI membranes by TEM analysis. The cross-section micrographs of SPI-N and SPI-B are shown in Fig. 8, in which the dark regions represent hydrophilic ionic domains and the bright regions refer to hydrophobic moieties. It is found that both SPI-N and SPI-B membranes exhibited clear microphase separation structures.

In the TEM micrographs of SPI-B membranes, a large amount of bigger ionic clusters (6–8 nm) and a certain amount of smaller ionic clusters (2–3 nm) were observed combined with medium size clusters. This is attributed to the twisted non-coplanar naphthalene structure in polymer backbone, which is favorable for the aggregation of hydrophilic sulfonic acid groups to form larger and smaller ionic clusters. On the contrary, the TEM micrographs of SPI-N membranes showed the spherical ionic clusters in a uniform distribution with the average size of 4–5 nm. The clusters were close to each other, which is favorable for water keeping and proton transport. This is the reason why SPI-N membranes exhibited better proton conductivities and high water uptakes than SPI-B membranes, although they were synthesized with the same sulfonation degree. Moreover, the hydrophilic domains in SPI-N1 and SPI-N2 seemed smaller and with better connectivity as comparing with SPI-N3. This is considered to be related to the hydrophobic trifluoromethyl groups in the polymer backbone, which is helpful to the formation of microphase separation structure. From the TEM observation combined with the proton conductivities of SPI membranes, it can be concluded that the good microphase separation structure is contribute to their better proton-conducting performance. The well-balanced properties of SPI membranes are promising candidates as proton exchange membrane for DMFC applications. The DMFC performance of these SPI membranes will be investigated in the future work and reported later.

4. Conclusions

A novel side-chain-type sulfonated aromatic diamine, 5-[1,1-bis (4-aminophenyl)-2,2,2- trifluoroethyl]-2-(4-sulfophenoxy)benzenesulfonic acid (BABSA), was synthesized and characterized. Two series of sulfonated polymides (SPI-N and SPI-B) were synthesized from six-membered dianhydrides NTDA or BNTDA, sulfonated aromatic diamine BABSA and various non-sulfonated aromatic diamines. These membranes displayed good solubility in many common organic solvents even in proton form because of the synergetic effects of the bulky aromatic pendant groups and the fluorinated substituents in the polymer structure. The flexible and strong sulfonated polyimide membranes SPI-N and SPI-B exhibited good dimensional stability with isotropic swelling less than 22% and high thermal stability with the desulfonation temperature of 283–330 °C. Their water stability is greatly affected by the flexibility of polymer main chain. These membranes also displayed excellent oxidation stability, which could be improved by the incorporation of trifluoromethyl groups in polymers backbone. All the SPI membranes have better permselectivity with the ratios of proton conductivity to methanol permeability (Φ) of nearly two to three times of that for Nafion 115. The SPI-N membranes based on NTDA showed much better proton conductivity and slightly higher methanol permeability than SPI-B membranes based on BNTDA because of the higher IEC values of the former, despite they have same sulfonation degree. The proton conductivities of SPI membranes were increased with temperature. The SPI-N membranes exhibited higher proton conductivity than Nafion 115 as the temperature over 40 °C and their σ values increased to 0.18–0.22 S/cm at 80 °C. The highly conducting performance of SPI-N membranes is attributed to their good hydrophobic/hydrophilic microphase separation structure.

References

[1] Hogarth MP, Hards GA. Platinum Met-Rev 1996;40(4):150–9.
[2] Zhang Y, Wan Y, Zhao C, Shao K, Zhang G, Li H, et al. Polymer 2009;50(19):4471–8.
[3] Zhai F, Guo X, Fang J, Xu H. J Membr Sci 2007;296:102–9.
[4] Okamoto K, Yin Y, Yamada O, Islam MN, Honda T, Mishima T, et al. J Membr Sci 2005;258(1–2):115–22.
[5] Mauritz KA, Moore RB. Chem Rev 2004;104(10):4535–86.
[6] Asano N, Aoki M, Suzuki S, Miyatake K, Uchida H, Watanabe M. J Am Chem Soc 2006;128(5):1762–9.
[7] Heinzel A, Barragán VM. J Power Sources 1999;84(1):70–4.
[8] Kreuer KD. J Membr Sci 2001;185(1):29–39.
[9] Gurau B, Smotkin ES. J Power Sources 2002;112(2):339–52.
[10] Hobson LJ, Nakano Y, Ozu H, Hayase S. J Power Sources 2002;104(1):79–84.
[11] DeLuca NW, Elabd YA. J Polym Sci Part A Polym Phys 2006;44:2201–25.
[12] Ye YS, Yen YC, Cheng CC, Chen WY, Tsai LT, Chang FC. Polymer 2009;50(14):3196–203.
[13] Jones DJ, Roziere J. J Membr Sci 2001;185(1):41–58.
[14] Chu PP, Wu CS, Liu PC, Wang TH, Pan JP. Polymer 2010;51(6):1386–94.
[15] Wang F, Hickner M, Kim YS, Zawodzinski TA, McGrath JE. J Membr Sci 2002;197(1–2):231–42.
[16] Miyatake K, Chikashige Y, Higuchi E, Watanabe M. J Am Chem Soc 2007;129:3879–87.
[17] Staiti P, Lufrano F, Aricò AS, Passalacqua E, Antonucci V. J Membr Sci 2001;188(1):71–8.
[18] Song JM, Miyatake K, Uchida H, Watanabe M. Electrochim Acta 2006;51:4497–504.
[19] Zou L, Roddecha S, Anthamatten M. Polymer 2009;50(14):3136–44.
[20] Somboonsub B, Invernale MA, Thongyai S, Praserthdam P, Scola DA, Sotzing GA. Polymer 2010;51(6):1231–6.
[21] Li N, Liu J, Cui Z, Zhang S, Xing W. Polymer 2009;50(19):4505–11.
[22] Genies C, Mercier R, Sillion B, Cornet N, Gebel G, Pineri M. Polymer 2001;42(2):359–73.
[23] Guo X, Fang J, Watari T, Tanaka K, Kita H, Okamoto K. Macromolecules 2002;35(17):6707–13.
[24] Meyer G, Perrot C, Gebel G, Gonon L, Morlat S, Gardette J-L. Polymer 2006;47(14):5003–11.
[25] Fang J, Guo X, Harada S, Watari T, Tanaka K, Kita H, et al. Macromolecules 2002;35:9022–8.
[26] Vallejo E, Pourcelly G, Gavach C, Mercier R, Pineri M. J Membr Sci 1999;160(1):127–37.
[27] Genies C, Mercier R, Sillion B, Petiaud R, Cornet N, Gebel G, et al. Polymer 2001;42(12):5097–105.
[28] Yin Y, Yamada O, Tanaka K, Okamoto K. Polym J 2006;38(3):197–219.
[29] Yin Y, Fang J, Watari T, Tanaka K, Kita H, Okamoto K. J Mater Chem 2004;14:1062–70.
[30] Hu Z, Yin Y, Kita H, Okamoto K, Suto Y, Wang H, et al. Polymer 2007;48:1962–71.
[31] Li N, Cui Z, Zhang S, Xing W. J Membr Sci 2007;295:148–58.
[32] Sutou Y, Yin Y, Hu Z, Chen S, Kita H, Okamoto K, et al. J Polym Sci Part A Polym Chem 2009;47(5):1463–77.
[33] Hu Z, Yin Y, Chen S, Yamada O, Tanaka K, Kita H, et al. J Polym Sci Part A Polym Chem 2006;44:2862–72.
[34] Chen K, Chen X, Yaguchi K, Endo N, Higa M, Okamoto K. Polymer 2009;50(2):510–8.
[35] Miyatake K, Zhou H, Matsuo T, Uchid H, Watanabe M. Macromolecules 2004;37:4961–6.
[36] Yan J, Liu C, Wang Z, Xing W, Ding M. Polymer 2007;48(21):6210–4.
[37] Mitchell RH, Lai Y-H, Williams RV. J Org Chem 1979;44(25):4733–5.
[38] Li N, Cui Z, Zhang S, Xing W. Polymer 2007;48:7255–63.
[39] Cao J, Wang Z. J Polym Sci Part A Polym Chem 1995;33:1627–35.
[40] Savard O, Peckham TJ, Yang Y, Holdcroft S. Polymer 2008;49(23):4949–59.
[41] Li N, Cui Z, Zhang S, Li S, Zhang F. J Power Sources 2007;172:511–9.
[42] Yin Y, Yamada O, Suto Y, Mishima T, Tanaka K, Kita H, et al. J Polym Sci Part A Polym Chem 2005;43:1545–53.
[43] Fang J, Guo X, Xu H, Okamoto K. J Power Sources 2006;159(1):4–11.
[44] Chen S, Yin Y, Kita H, Okamoto K. J Polym Sci Part A Polym Chem 2007;45(13):2797–811.
[45] Qiu Z, Wu S, Li Z, Zhang S, Xing W, Liu C. Macromolecules 2006;39(19):6425–32.
[46] Watari T, Fang J, Tanaka K, Kita H, Okamotoa K, Hirano T. J Membr Sci 2004;230:111–20.